ORIGINAL RESEARCH

Amalgamation of complex iron(III) ions and iron nanoclusters with MWCNTs as a route to potential T_2 MRI contrast agents

Nikodem Kuźnik[1]
Mateusz M Tomczyk[1]
Marzena Wyskocka[1]
Łukasz Przypis[1]
Artur P Herman[1]
Rafał Jędrysiak[1]
Krzysztof K Koziol[2]
Sławomir Boncel[1]

[1]Department of Organic Chemistry, Bioorganic Chemistry and Biotechnology, Faculty of Chemistry, Silesian University of Technology, Gliwice, Poland; [2]Department of Materials Science and Metallurgy, University of Cambridge, Cambridge, UK

Correspondences: Nikodem Kuźnik; Sławomir Boncel
Department of Organic Chemistry, Bioorganic Chemistry and Biotechnology, Faculty of Chemistry, Silesian University of Technology, Krzywoustego 4, 44-100 Gliwice, Poland
Tel +48 32 237 1839; +48 32 237 2353
Fax +48 32 237 2094
Email nikodem.kuznik@polsl.pl; slawomir.boncel@polsl.pl

Abstract: Iron-filled multiwall carbon nanotubes (Fe@MWCNTs) were functionalized toward a variety of potential magnetic resonance imaging contrast agents. Oxidized Fe@MWNCTs were covered with PEG5000 via direct esterification or using acyl chloride derivatives. Alternatively, the latter were functionalized with an aminophenol ligand (Fe@O-MWCNT-L). Moreover, pristine Fe@MWCNTs were functionalized with N-phenylaziridine groups (Fe@f-MWCNT) via [2+1] cycloaddition of nitrene. All of these chemically modified nanotubes served as a vehicle for anchoring Fe^{3+} ions. The new hybrids – Fe(III)/Fe@(f-/O-)MWCNTs – containing 6%–14% of the "tethered" Fe^{3+} ions were studied in terms of the acceleration of relaxation of water protons in nuclear magnetic resonance. The highest transverse relaxivity r_2=63.9±0.9 mL mg^{-1} s^{-1} was recorded for Fe(III)/Fe@O-MWCNT-L, while for Fe(III)/Fe@f-MWCNT, with r_2=57.9±2.9 mL mg^{-1} s^{-1}, the highest impact of the anchored Fe(III) ions was observed. The T_1/T_2 ratio of 30–100 found for all of the nanotube hybrids presented in this work is a very important factor for their potential application as T_2 contrast agents. Increased stability of the hybrids was confirmed by ultraviolet–visible spectrophotometry.

Keywords: multiwall carbon nanotubes, Fe^{3+}, transverse relaxation time T_2, MRI contrast agent

Introduction

Carbon nanotubes (CNTs), since their rediscovery,[1,2] have raised a lot of interest among scientists, providing ample opportunities of potential and already marketed everyday applications. Investigations into the new territory have been launched, and the large diversity of seemingly simple tubes is under continuous exploration. Both diagnostic and therapeutic medical applications of CNTs have driven an enthusiastic attention.[3,4] However, until previous uncertainties concerning CNTs' prolonged in vivo cytotoxicity as well as relationships between their potential toxicity and 1) morphology/surface chemistry, 2) administration routes, and 3) efficiency of harmless excretion are fully dispelled, the international scientific society cannot cross the threshold of the first medical application.[5–7]

Since the past several years, CNTs have emerged as new candidates for applications in medical imaging and, currently, this is one of the most attractive fields of scientific investigations.[8,9] Magnetic resonance imaging (MRI), as a noninvasive technique, is applied worldwide and takes on ever-new forms using the developments in computer technology and by enhancing/refining the image with contrast agents (CAs). Classical CAs are magnetic substances affecting the relaxation mechanism (transition from the excited into the ground state) of water protons in strong magnetic fields.

Relaxation of protons has two independent components; hence, it is a tour de force challenge to accelerate only one of them. Gadolinium complexes are currently applied in routine medical practice as longitudinal T_1 CAs, leading to brightening of the image in the region of their accumulation. On the other hand, superparamagnetic iron oxide nanoparticles (SPIONs) are transverse, negative T_2 CAs. According to the Bloembergen theory, on a molecular level, the acceleration mechanism proceeds by direct interaction of the proton with the magnetic center, called the inner sphere mechanism.[10] If the relaxing water proton is in the resultant field of the magnetic materials, an outer sphere mechanism takes place and it is an r^6-order effect. CNTs, especially those obtained by catalytic methods, often include metallic nanoparticles (formed by decomposition of, eg, ferrocene) as precursors of nanotube growth.[11] As a consequence, iron (and iron-based phases) nanoparticles can be encapsulated in multiwall carbon nanotubes (MWCNTs) produced by catalytic chemical vapor deposition (c-CVD), leading to ferromagnetic and/or superparamagnetic properties.[12] For this reason, one could portray the nanoparticulate iron designating the pristine nanomaterial as Fe@MWCNT. Furthermore, CNTs expand their applicability by functionalization. Oxidizing the nanotube surface at the most reactive graphene defects (nanotube cap regions, Stone–Thrower–Wales defects, irregularities, waviness, kinks, etc),[13] additionally accelerated by digestion of the CNT wall fragments, by the action of classical oxidizing agents (HNO_3/H_2SO_4) leads to the introduction of carboxylic and hydroxyl groups and formation of Fe@O-MWCNTs. This modification opens new possibilities of anchoring organic, polymeric, or metallic moieties on the scaffold. Such an approach has recently let us to report Fe@O-MWCNTs with anchored Fe(III) ions (Fe(III)/Fe@O-MWCNT), which accelerated the T_2 relaxation of water protons successfully, although the effect varied with the strength of the magnetic field.[14] Furthermore, some other groups have explored similar ideas on the applications of CNTs as MRI CAs,[15,16] and a variety of CNT types has been studied: ultrashort CNTs (US-CNTs),[17–19] single-wall (SWCNTs),[20–22] and MWCNTs.[23–26] However, approaches and targets both differed: 1) SPIONs were immobilized via ionic interactions between poly(diallyldimethylammonium)-pretreated oxidized CNTs and lactose-glycine covered Fe_3O_4 nanoparticles ("indirect" approach),[27,28] or 2) iron-based nanoparticles were produced in situ as "corks" for HiPCO CNTs ("direct" approach);[21,24] the nanotubes were additionally functionalized mainly with polymers. On the basis of our recent experience with Fe^{3+}-nanotube complexes

as relaxation accelerators, we decided to explore this field further. As a continuation of our studies, we present here comprehensive physicochemical studies on the potential application of various Fe(III)/Fe@MWCNT hybrids as T_2 CAs. Obviously, the sine qua noncondition is to prepare and further apply noncytotoxic hybrids. In this aspect, we were encouraged by our studies, which revealed that Fe@O-MW-CNTs were found as fully water-dispersible nanoparticles (with a dispersion stability over several months) and were nontoxic against human monocyte-derived macrophages within 48 hours of incubation.[29] Other recently published works have also played an encouraging role in our studies, especially when concerning polyethylene glycol-modified (PEGylated) individualized nanotubes exhibiting prolonged dispersibility in water and minimal cytotoxicity in vivo in mice.[30,31]

Results and discussion

Fe@MWCNTs were synthesized by c-CVD using a known procedure.[32] Fe@O-MWCNTs were prepared from pristine Fe@MWCNTs refluxed in a mixture of concentrated sulfuric and nitric acids as described previously.[14] According to elementary analysis and thermogravimetric analysis (TGA) (Fe content as calculated per Fe_2O_3 after complete combustion of the sample), pristine and oxidized nanotube vehicles (as precursors of functionalization) had the elemental composition presented in Table 1. Iron nanoparticles present in the nanotube material were of postcatalytic origin as incorporated into the nanotube inner cavities by the c-CVD method.

Functionalization of Fe@(O-/f-) MWCNTs

On the basis of our previous results, we first designed two modifications of Fe@O-MWCNTs (Figure 1). Primarily, nanotubes were covalently PEGylated (product of PEGylation denoted as Fe@O-MWCNT-PEG further in the text), which could enhance the hydrophilicity and dispersibility (and hence mobility) in biofluids as well as inhibit possible future immunological reactions of the hybrids and

Table 1 Composition of Fe@O-MWCNTs

Element	Content (%) (weight/weight)	
	Fe@MWCNTs	Fe@O-MWCNTs
Fe	2.6	2.2±0.5
C	97.4	86.5±0.1
H	0.0	0.15±0.09
O	0.0	11.15±3.23

Abbreviations: Fe@MWCNT, iron-filled multiwall carbon nanotube; Fe@O-MWCNT, oxidized Fe@MWCNT.
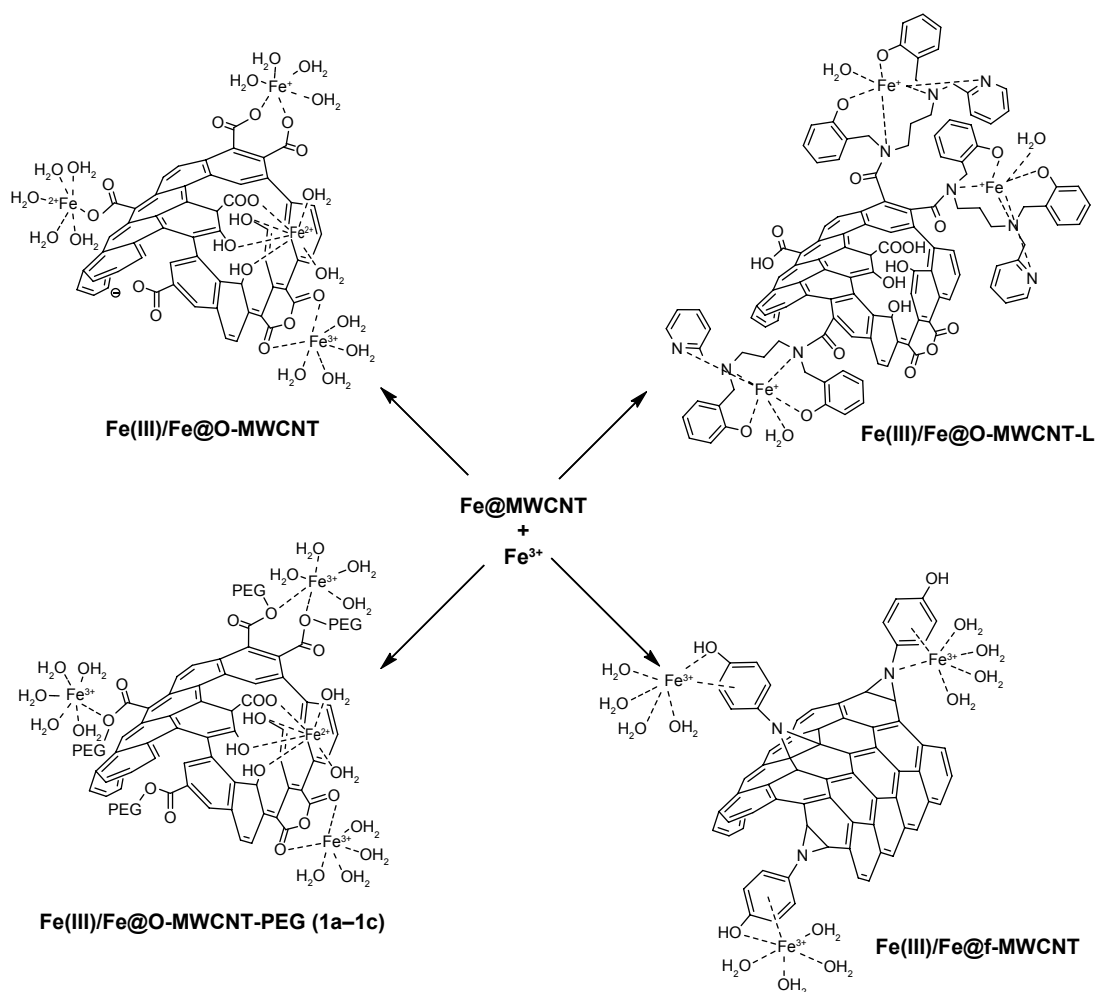
Figure 1 Modification of Fe@MWCNTs.

Notes: For clarity, only the outer nanotube wall is shown indicating oxidation defects as gaps and corresponding functional groups; the descriptions **1a–1c** correspond to the appropriate products obtained through different synthetic routes.

Abbreviations: Fe@MWCNT, iron-filled multiwall carbon nanotube; Fe@O-MWCNT, oxidized Fe@MWCNT; Fe@f-MWCNT, Fe@MWCNT functionalized with *N*-phenylaziridine groups; L, *N,N,N′*-[bis(2-hydroxyphenylmethyl)]-[(2-pyridinyl)methyl]-1,3-propanediamine ligand; PEG, polyethylene glycol.

enhance their clearance.[33] The second modification was designed to equip the Fe@O-MWCNTs with an organic moiety (L) responsible for strong coordination with Fe^{3+} ions (Fe@O-MWCNT-L). As the third studied nanotube hybrid, pristine Fe@MWCNTs were functionalized with *N*-phenylaziridine groups (Fe@f-MWCNT) via [2+1] cycloaddition of nitrene (generated in situ from the corresponding azide).[34] These hybrids were expected to have a high affinity to Fe^{3+} because phenol complexes are known for their typically large values of stability constants (K).[35]

We applied three different approaches to synthesize Fe(III)/Fe@O-MWCNT-PEG (Figure 2). The first approach (**1a**) was based on a direct reaction between Fe@O-MWCNT and hydroxyl PEG (PEG-OH) without any solvent.[36] The reaction was carried out in an excess of molten PEG-OH (melting point =59°C) at 100°C. These conditions were

advantageous for a shift of the esterification equilibrium toward the formation of ester because of evaporation of water during the process. Separation of the unreacted glycol was achieved by washing out with a series of organic solvents (benzene, tetrahydrofuran, diethyl ether). After drying by lyophilization, ultraviolet–visible (UV–Vis) spectra of the resulting hybrids were acquired and compared with the spectra of substrates. Absorption maximum was shifted from 232 nm to 270 nm, which corresponds to the transformation of carboxyl groups to new species.[37] This band cannot be assigned to free PEG-OH in the postreaction mixture as it yields much weaker absorption band at 268 nm.

The second approach (**1b**) was based on a reverse sequence of the above reactions, ie, here, iron-enriched Fe(III)/Fe@O-MWCNTs (the synthesis has been published
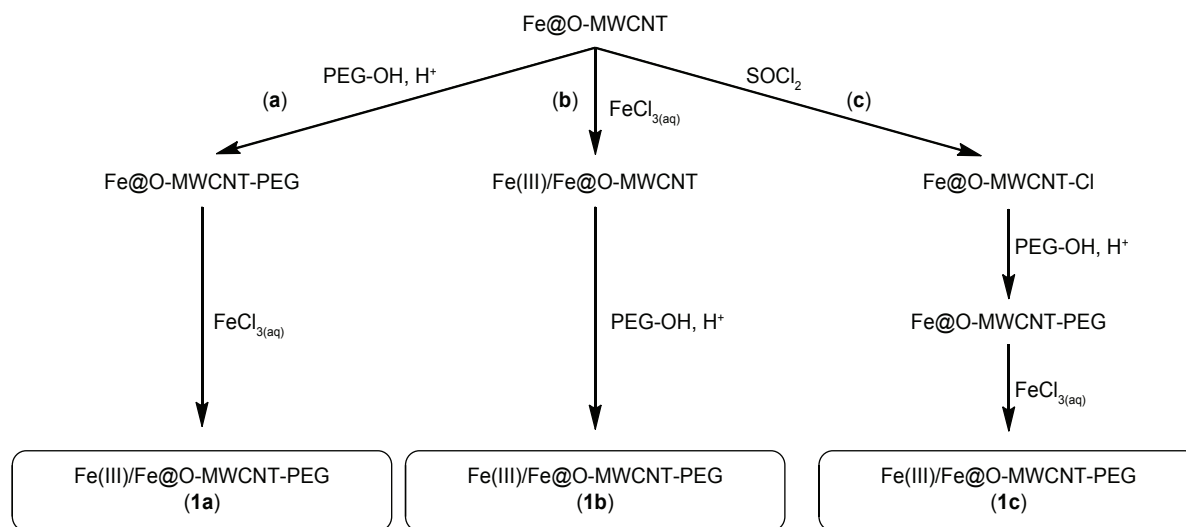
Figure 2 Three different approaches to synthesize Fe(III)/Fe@O-MWCNT-PEG (**1a–1c**).
Abbreviations: Fe@MWCNTs, iron-filled multiwall carbon nanotubes; Fe@O-MWCNT, oxidized Fe@MWCNT; FeCl$_3$, ferric chloride; PEG, polyethylene glycol; PEG-OH, hydroxyl PEG; SOCl$_2$, thionyl chloride.

before[14] and is described in detail further in the text) were subjected to reaction with PEG-OH.

Finally, the last method (**1c**) consisted of two steps: 1) transformation of the hydroxyl groups from Fe@O-MW-CNT (both carboxylic and phenolic) to a more reactive chloro derivative (Fe@O-MWCNT-Cl) by treatment with thionyl chloride, followed by 2) reaction with PEG-OH. This method is a modification of Chen et al's procedure.[38] Fe@O-MWCNTs were heated in excess of thionyl chloride with *N,N*-dimethylformamide as solvent; the unreacted SOCl$_2$ was distilled off. The residue was washed with anhydrous tetrahydrofuran and applied immediately to further transformations. The following reaction with PEG-OH was carried out in molten PEG-OH for 96 hours. According to Chen et al, elevated temperature and prolonged reaction time are necessary for the successful functionalization.[38] The efficient purification of the Fe@O-MWCNT-PEG hybrid in this case was achieved by suspension of the reaction mixture in ethanol and centrifugation of the product. UV–Vis spectra of this material revealed clear bathochromic shift of the absorbance maximum from 232 nm to 270 nm, which stands for the functionalization of hydroxyl (including carboxylic) groups with the formation of PEG esters and ethers. TGA (Supplementary materials) has shown that the material (**1a–1c**) was loaded with 20–25 wt% of PEG.

Fe@O-MWCNT-L was synthesized in the reaction of Fe@O-MWCNT-Cl with *N,N,N'*-[bis(2-hydroxyphenylmethyl)]-[(2-pyridinyl)methyl]-1,3-propanediamine (L)[39] – an *N,O*-ligand with a secondary amine group. The reaction was carried out in boiling dichloromethane, and the excess of organic compounds

was washed out with methanol. UV–Vis spectra of the product (Fe@O-MWCNT-L) showed an evident transformation, reflected by the emergence of a strong absorption band at 274 nm that was absent in the substrate.

Fe@f-MWCNT was synthesized by reacting pristine Fe@MWCNTs with *p*-azidophenol in 1,1,2,2-tetrachloroethane under reflux in an inert atmosphere. To achieve high functionalization degree, Fe@MWCNTs were sonicated before the addition of *p*-azidophenol. Solid product of the reaction was washed with large amounts of chloroform, toluene, and methanol to ensure that neither unreacted *p*-azidophenol nor possible side products[40] were adsorbed physically on the material. It was found that the use of 1,1,2,2-tetrachloroethane (boiling point of 146.5°C) as a solvent is crucial for thermal decomposition of the azide moiety. The degree of functionalization was determined by TGA and it was assessed as 9% (w/w) of >N–Ph–OH groups.

Specifications and stability of hybrids

Functionalization of Fe@MWCNTs was manifested by the appearance of new absorption bands in UV–Vis characteristics for the newly formed and/or introduced moieties. For Fe@O-MWCNTs, the most intensive absorption band derives from carboxylic groups localized in the range of 230–234 nm (benzoic acid has an absorption maximum at 230 nm). These results prompted us to assess the homogeneity and stability of the source materials, ie, Fe@O-MWCNTs. Therefore, UV–Vis spectra were acquired for four different batches of Fe@O-MWCNTs prepared in identical manner, and excellent homogeneity of the samples and
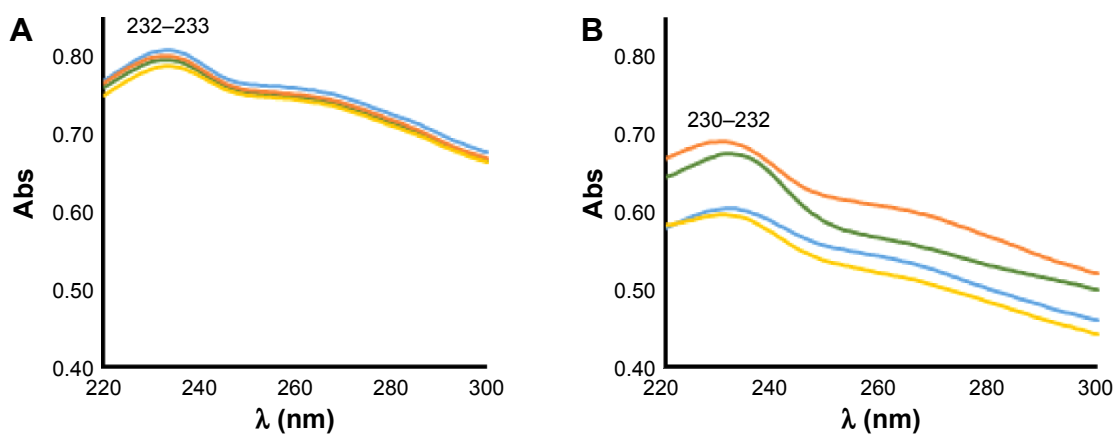
Figure 3 UV–Vis spectra of four Fe@O-MWCNT batches right after sonication (**A**), and 2 months later (**B**).
Note: The different lines represent different batches.
Abbreviations: Abs, absorbance; Fe@O-MWCNT, oxidized Fe@MWCNT; Fe@MWCNT, iron-filled multiwall carbon nanotube; UV–Vis, ultraviolet–visible.

satisfactory reproducibility of the preparation procedure was found. Spectra in Figure 3A show only insignificant deviations in the absorption among the four samples recorded immediately after sonication in water (samples of 0.5 mg CNTs per 5 mL H_2O, spectra were recorded in the range of 220–300 nm).

Additionally, 2-month observation revealed minor differences in the stability of dispersions and minor hypsochromic shift of the absorption maximum (from 233–234 nm to 230–232 nm) (Figure 3B). This behavior, observed also by Cheng et al[41] is based on the relative change in the contribution of nanotubes of different lengths and different degrees of functionalization remaining in the dispersion.

To compare the stability of the functionalized nanotubes, we recorded the UV–Vis spectra of the nanotube dispersions within the first 24 hours after sonication (Table 2). To eliminate the effect of surfactants, we prepared the dispersions in demineralized water. The most reliable wavelength common for all the nanotube hybrids was 400 nm, because as mentioned earlier, the absorption near the maxima could fluctuate.

Table 2 Sedimentation degree of MWCNTs within 24 hours

Fe@(O-/f-)MWCNTs	Decrease in the stability of nanotube hybrid dispersions [absorbance/hour] in the first 24 hours
Fe@O-MWCNT	0.0049
Fe@O-MWCNT-PEG (1a–1c)	0.0002–0.0008
Fe@O-MWCNT-L	0.0097
Fe@f-MWCNT	0.0147

Abbreviations: Fe@MWCNT, iron-filled multiwall carbon nanotube; Fe@O-MWCNT, oxidized Fe@MWCNT; Fe@f-MWCNT, Fe@MWCNT functionalized with *N*-phenylaziridine groups; L, *N,N,N′*-[bis(2-hydroxyphenylmethyl)]-[(2-pyridinyl)methyl]-1,3-propanediamine ligand; PEG, polyethylene glycol.

The results clearly demonstrated that covering Fe@O-MWCNT with nonionized polymers such as PEG increased the suspension stability several times (with reference to the source Fe@O-MWCNT). The source material exhibited high stability due to the presence of numerous polar carboxyl, hydroxyl, and carbonyl fragments. Its modification with aminophenol ligand (Fe@O-MWCNT-L) decreased hydrophilicity, leading to a higher rate of sedimentation. Simultaneously, the alternative approach based on a direct introduction of phenol moieties via the aziridine derivative (Fe@f-MWCNT) resulted in the least stable dispersion. Additional enhancement of stability was observed in the case of sodium dodecylbenzenesulfonate (SDBS)-supported nanotube dispersions, in which there was no visual sedimentation for several months (not included in Table 2).

Anchoring Fe^{3+} ions

CNTs as adsorbents with large specific surface areas exhibit a high affinity to metal ions. Sitharaman et al[17] used US-CNTs as gadolinium ion sponges and then studied the hybrids as T_1 CAs. High longitudinal relaxivity r_1 was found, reaching 173 mM s^{-1} at 1.4 T. An even higher relaxivity was recorded for lower magnetic fields, but it has no practical use for the current MRI devices. Because gadolinium is a poorly efficient T_2 accelerator, it is not surprising that authors did not report these results. Recently, Maragon et al[42] reported relaxivities of r_1=4.1 mM s^{-1} and r_2=4.6 mM s^{-1} for Gd^{3+} anchored onto MWCNT via amino-carboxylic ligands in the range of 1–5 T. Our recent studies indicated a high potential of Fe^{3+} ions as T_1 accelerators in classical coordination complexes,[43,44] but we were also surprised with the efficiency in accelerating transverse relaxation (T_2) when anchored onto Fe@O-MWCNT.[14] Moreover, our findings showed a high selectivity

of T_2 acceleration relative to T_1, which is a crucial factor for T_2 CAs. For this reason, we have expanded the field of our studies to other Fe-MWCNT hybrids. We have modified Wilson's procedure (applied initially for Gd^{3+} ions) of Fe^{3+} adsorption on MWCNTs described earlier. The procedure of adsorption was based on the expected coordination potential. Then, the free Fe^{3+} ions were washed out by consecutive steps of preparing dispersion and centrifugation. In the third cycle of dispersion/centrifugation, free Fe^{3+} content in the supernatant was found below the detection limit in the rhodanide test. The 1,10-phenanthroline test (detection limit: 0.8 ppm) confirmed these results. On the other hand, free Fe^{3+} content in the supernatants from the two initial washings let us assess the amount of Fe^{3+} adsorbed on nanotubes (Table 3). We also observed that the critical parameter in the washing procedure was temperature of the centrifugation. For example, the product formed in the **1c** route was very difficult to separate after 10 minutes of centrifugation (10,000 rpm) at room temperature, but lowering the temperature to 4°C yielded a clear supernatant.

Iron(III) anchoring proved to be successful, as shown by both UV–Vis quantitative determination as well as the resulting properties described later as the essence of this work. Iron(III) content reached 6%–14% weight/weight [iron(III) per weight of the hybrid]. The 4-(aziridin-1-yl)phenol-functionalized nanotubes, ie, Fe@f-MWCNTs, were the least Fe^{3+}-loadable vehicles. It is possible that the strategy of surface functionalization gave less coordination sites than the regular harsh oxidation applied initially to all other pristine Fe@MWCNTs. It is likely that the phenol substituents were not located close to each other, thus chelating coordination was not common on this surface. Moreover, nitrene molecule can undergo subsequent and competitive reactions, lowering the total number of accessible sites for coordination (eg, formation of azepines, etc). Contrarily, oxidation of the nanotube surface disrupted several neighboring positions, forming numerous new coordination sites. It is interesting to note that iron(III) anchoring was found to be independent of the method of PEGylation (**1a**–**1c**), and additionally, the presence of long PEG chains did not hamper the introduction of iron ions, which could be potentially possible by transforming the ionic carboxylic groups into nonionic esters. Iron ions neither gained higher affinity to PEG-covered nanotubes. On the other hand, the effect of introduction of a typical ligand (Fe@O-MWCNT-L) is clearly visible by the increase of iron affinity resulting in the iron content being more than 40% higher than in any other case.

Relaxation measurements

As we have already reported, we observed a high potential of Fe(III)/Fe@O-MWCNT in the acceleration of transverse relaxation time T_2 of water protons. Therefore, we were surprised by even higher values of relaxivity for the proposed nanotube hybrids (Table 4).

Initially, introduction of PEG (entry 3, Table 4) lowered the relaxivity of nanotubes relative to the source material (entry 1). This behavior might result from wrapping of the nanotube surface by the polymer chains, hampering interaction of water molecules with the coordinating surface. Because the acceleration effect is governed by short distance forces (r^6), water protons "felt" weaker magnetic field from the encapsulated iron nanoparticles and thus relaxed more slowly. Nevertheless, the acceleration was found to be already very high because simple Fe^{3+} was inefficient in this regard (entry 11). However, the introduction of Fe^{3+} ions onto the PEG-derived nanotubes (entries 4–6) showed an effect similar to that of non-PEG-covered nanotubes (entry 2). Therefore, the introduced iron ions gave an additional impact to relaxivity, but the procedure of ultrasonication might also unwrap/loosen to some extent the tubes from the PEG tails and hence enable a better access of water molecules to the surface. Additionally, in the latter case, the presence of polar polyether moieties enhanced the penetration of PEG chains by water of the nanotube surfaces, resulting in a higher rate of exchange of water molecules.[33] It is important to recall here the much higher stability of the PEG derivatives compared to the non-PEG-covered Fe@O-MWCNTs (Table 2).

A striking increase in the relaxivity was observed for nanotubes functionalized with the aminophenol ligand – Fe@O-MWCNT-L (entry 7). The small organic molecule apparently did not hinder but even intensified interactions of water with nanotubes. Critically, an increase of >40%

Table 3 The effect of Fe^{3+} anchoring onto Fe@(f-/O-)MWCNTs

Hybrid	Mass of Fe^{3+} adsorbed on 1 g of nanotubes (mg)	Fe^{3+} content (m/m%)
Fe(III)/Fe@O-MWCNT	120	10.7
Fe(III)/Fe@O-MWCNT-PEG (**1a**)	118	10.6
Fe(III)/Fe@O-MWCNT-PEG (**1b**)	101	9.9
Fe(III)/Fe@O-MWCNT-PEG (**1c**)	124	11.0
Fe(III)/Fe@O-MWCNT-L	167	14.3
Fe(III)/Fe@f-MWCNT	66	6.2

Abbreviations: Fe@MWCNT, iron-filled multiwall carbon nanotube; Fe@O-MWCNT, oxidized Fe@MWCNT; Fe@f-MWCNT, Fe@MWCNT functionalized with *N*-phenylaziridine groups; L, *N,N,N′*-[bis(2-hydroxyphenylmethyl)]-[(2-pyridinyl)methyl]-1,3-propanediamine ligand; PEG, polyethylene glycol; MWCNT, multiwall carbon nanotube.

Table 4 Relavity r_2 of MWCNT-based magnetic hybrids as potential T_2 CAs

Entry	Hybrid	r_2 [(mg/mL)$^{-1}$ s^{-1}], 7.1 T, 22°C	Medium impact, $1/T_2$ [s^{-1}]	Medium
1	Fe@O-MWCNT	25.1±1.1	2.1	A
2	Fe(III)/Fe@O-MWCNT	34.4±5.0	3.2	A
3	Fe@O-MWCNT-PEG (**1a**)	13.6±2.6	1.8	B
4	Fe(III)/Fe@O-MWCNT-PEG (from **1a**)	41.1±2.7	2.3	B
5	Fe(III)/Fe@O-MWCNT-PEG (from **1b**)	36.6±0.3	0.8	B
6	Fe(III)/Fe@O-MWCNT-PEG (from **1c**)	36.5±1.9	0.1	B
7	Fe@O-MWCNT-L	44.8±0.7	1.0	B
8	**Fe(III)/Fe@O-MWCNT-L**	**63.9±0.9**	**1.0**	**B**
9	Fe@f-MWCNT	26.1±1.1	1.3	A
10	Fe(III)/Fe@f-MWCNT	57.9±2.9	1.3	A
11	FeCl$_3$	0.4±0.2	0.2	B

Notes: Medium A contains 1% (m/v) SDBS in 5% (v/v) D$_2$O in H$_2$O; B contains 5% (v/v) D$_2$O in H$_2$O. The bolded row is the row with the highest value of r_2.
Abbreviations: Fe@MWCNT, iron-filled multiwall carbon nanotube; Fe@O-MWCNT, oxidized Fe@MWCNT; Fe@f-MWCNT, Fe@MWCNT functionalized with N-phenylaziridine groups; L, N,N,N′-[bis(2-hydroxyphenylmethyl)]-[(2-pyridinyl)methyl]-1,3-propanediamine ligand; PEG, polyethylene glycol; MWCNT, multiwall carbon nanotube; CA, contrast agent; SDBS, sodium dodecyl benzenesulfonate.

in relaxivity was observed after Fe^{3+} anchoring (entry 8), resulting in the highest relaxivity in the studied series recorded, it must be emphasized, in the absence of surfactant (medium B).

Functionalization of MWCNTs with the aziridine–phenol groups resulted in similar relaxivity r_2. However, such an approach opened a route to Fe^{3+} anchoring with a >120% increase in the relaxivity. Such a leap of relaxivity by the introduction of Fe^{3+} was observed in the case of Fe(III)/Fe@O-MWCNT-PEG, but the factor of PEG unwrapping must be taken into account according to studies by Xu's group[33] and Welsher et al.[45]

It is also interesting to consider the changes in relaxivity of functionalized nanotubes and products of Fe^{3+} anchoring thereto with respect to the efficiency of anchoring (Tables 3 and 4). In the case of Fe@O-MWCNT and Fe@O-MWCNT-PEG (**1a**–**1c**), the final Fe^{3+} content was approximately 10%, but the increase in relaxivity after the anchoring was 40% (in the first case) and almost 300%, respectively. The tendency of wrapping could stand for this second case.[33] While the small organic aminophenol ligand L gave the best efficiency in Fe^{3+} anchoring, the amphiphilic nature of the ligand was also the most successful in the enhancement of water molecules' interaction with the surface and with the paramagnetic Fe^{3+} ions. Contrarily, the least effective in ion anchoring, the aziridine phenol derivative Fe@f-MWCNT (only 6 wt% of Fe^{3+}), yielded results in relaxivity comparable to those with Fe(III)/Fe@O-MWCNT-L. The relaxivity r_2 presented in Table 4 was calculated on weight of the product mass per amount of medium. It is a useful method to give an image of the weight of the entire product, giving appropriate effect of relaxation acceleration. However, in many research works, this magnitude was expressed in units per

millimole per second, so taking into account the introduced components (easily calculated per mole) onto the nanotubes. This is how such a representation gives an idea of the "value added" effect. Applying this approach here, eg, the relaxivity r_2 63.9 (mg/mL)$^{-1}$ s^{-1} for entry 8 would have to be recalculated to 25.0 mM^{-1} s^{-1} because of the high Fe(III) content, while for the entry 10 – due to the lowest efficiency in the iron(III) anchoring – r_2 would be equal to 52.1 mM^{-1} s^{-1} after recalculation. These values are already higher and comparable to the values for CNTs already reported by others (4–58 mM^{-1} s^{-1}).[20,23,42,46] However, there are still records that have not been beaten yet (180–360 mM^{-1} s^{-1}).[24,26,27,47]

It must be highlighted that we have undertaken additional studies to assess the behavior of the products in biological media. For this purpose, we have recorded relaxivity of the first candidate Fe(III)/Fe@O-MWCNT in different media of various acidities. We have prepared the appropriate dispersions in saline (0.9% NaCl) and in phosphate buffer (PB 0.1 M, pH 7.5). The resulting dispersions (with 1% SDBS) had pH values of 4.95 and 7.44, respectively. Then we have measured relaxivity of these dispersions, obtaining even higher relaxivities (r_2) reaching 70 mL s^{-1} mg^{-1} at 7.1 T and 22°C. Additionally, we have performed similar measurements in bovine serum, obtaining r_2=54 s^{-1} mg^{-1} at 7.1 T and 22°C. The results of the measurements yielded reproducible values. It is also important to emphasize that the dispersions were stable for several days (except for the PB dispersion, due to its high ionic strength). These results constitute a strong premise toward the high potential of other Fe-nanotube hybrids also because of the high values of relaxivity and excellent stability of dispersions (especially in the presence of surfactants). It is worth noting that their stability in terms of repeatable results in various media of different pH values,

although the obtained characteristics disables them from functioning as smart CAs (contrary to the gadonanotubular T_1 CAs),[48] denotes their predictable behavior under complex biological conditions.

We have measured T_1 relaxation of the water protons in the hybrid dispersion products, but we have observed neither acceleration nor detectable dependence of the products' concentrations on the relaxation rate of water protons. Moreover, the relaxation time was found to be in the range of 3 seconds–5 seconds, which is longer than that for distilled water (close to 3 seconds, depending on the conditions). It is not surprising because relaxation is also a function of water mobility, viscosity, and density of the medium. As T_2 of the most diluted dispersions (0.01 mg cm^{-3}) was close to 0.3 seconds and was 0.03 seconds for the most concentrated ones, the ratio T_1/T_2 is 30–100 for all of the hybrids described in the work. This is a very important factor for the potential application as T_2 CAs and is a unique parameter in comparison to the other already-reported CNT-based candidates.[21]

Materials and methods

All chemicals were obtained from commercial suppliers (Acros, Aldrich, Avantor). *N,N,N′*-[bis(2-hydroxyphenylmethyl)]-[(2-pyridinyl)methyl]-1,3-propanediamine (L) was obtained according to the procedure described previously.[39] For preparation of dispersion and washing, demineralized water of conductivity 0.075 µS cm^{-1} was used. UV–Vis spectra were taken on Hitachi Y-2910 spectrophotometer in the 190–700 nm range in aqueous solutions. Measurements were carried out using Mettler Toledo TGA/DSC 2 system. Analyses were conducted at constant heating rate of 10°C min^{-1}; inert gas (argon) flow rate was 80 mL min^{-1}, and 70 µL alumina crucibles were used. Relaxation measurements (7.1 T) were conducted on a Varian Unity Inova 300 MHz spectrometer at 22°C. Dispersions of the following concentrations were measured: 0.2 mg mL^{-1}, 0.1 mg mL^{-1}, 0.05 mg mL^{-1}, 0.001 mg mL^{-1}. The basic medium was 5% D$_2$O in demineralized water; however, in some cases, 1% (m/v) SDBS was added (Table 4). The measurements were repeated twice, and an average was taken for further calculations. Relaxivity r_2 was calculated as a slope of T_2 vs concentration (mg cm^{-3}) with pure medium as an intercept (reference point). Special attention was paid to the optimal shimming of the samples because nanotube dispersions give very broad proton signals on ^{1}H-nuclear magnetic resonance due to their ferromagnetic and superparamagnetic behaviors, as well as high viscosity. Long time (1–3 hours) acquisitions were not disrupted by sedimentation of the products. T_1 was

determined using infrared sequence with d_1=15 seconds and d_2=0.05 second, 0.1 second, 0.5 second, 0.75 second, 1 second, and 3 seconds. T_2 was determined using Carr-Purcell-Meiboom-Gill (CPMG) sequence with d_1=8 seconds, d_2=0.01 seconds, and bt=0.01 second, 0.05 second, 0.1 second, 0.5 second, 1 second, 2 seconds, and 4 seconds.

Fe@O-MWCNT-PEG (1a)

Into a round-bottom flask, 500 mg of PEG$_{5,000}$ (~0.1 mmol) was introduced and molten on an oil bath, followed by the addition of 50 mg Fe@O-MWCNT. After 10 minutes of heating, few drops of concentrated H$_2$SO$_4$ were added, and the reaction mixture was heated for 2 hours at 100°C. After cooling, 5 mL of benzene was added, and the postreaction mixture was filtered on a fritted funnel equipped with a poly-tetrafluoroethylene (PTFE) filter, then washed with diethyl ether, tetrahydrofuran, acetone, water, and again acetone until a colorless filtrate was obtained. The wet semisolid was lyophilized, yielding 26 mg of dry solid.

Fe@O-MWCNT-PEG (1b)

Into a round-bottom flask, 500 mg PEG$_{5,000}$ (~0.1 mmol) was introduced and molten on an oil bath, followed by the addition of 38 mg Fe(III)/Fe@O-MWCNT. After 10 minutes of heating, few drops of concentrated H$_2$SO$_4$ were added and heated for 2 hours at 100°C. After cooling, 5 mL of benzene was added, and the postreaction mixture was filtered on a fritted funnel equipped with a PTFE filter, then washed with diethyl ether, tetrahydrofuran, acetone, water, and again acetone until a colorless filtrate was obtained. The wet gunk was lyophilized, yielding 27 mg of dry solid.

Fe@O-MWCNT-Cl

Into a round-bottom flask, 916 mg of Fe@O-MWCNT (lyophilized before use), 9 mL (0.124 mol) of freshly distilled SOCl$_2$, and 1 mL of anhydrous dimethyl formamide were introduced. The reaction mixture was heated under inert atmosphere for 8 hours in an oil bath at 70°C with magnetic stirring. The next portion of SOCl$_2$ was added (15 mL, 0.207 mmol) and the heating was continued for the next 16 hours. Afterward, the excess of unreacted SOCl$_2$ was distilled off, and 40 mL of tetrahydrofuran was added to the residue to filter it off on a PTFE filter. The semisolid was dried under reduced pressure under inert atmosphere, yielding 825 mg of dry product.

Fe@O-MWCNT-PEG (1c)

Into a round-bottom flask, 10 g of PEG5000 (~2 mmol) was introduced and molten on an oil bath, followed by the addition

of 200 mg Fe@O-MWCNT-Cl. The reaction mixture was heated under inert atmosphere for 96 hours at 100°C on an oil bath with magnetic stirring. The so-formed hard solid was crushed and washed on a PTFE filter with ethanol until a colorless filtrate was obtained. The solid was then suspended in 40 mL of ethanol and centrifuged (12,000 rpm for 15 minutes, room temperature). The precipitate was dried under reduced pressure, then suspended in water, and lyophilized, yielding 188 mg of product.

Fe@MWCNT-L

Into a round-bottom flask, 700 mg (1.85 mmol) of N,N,N'-[bis(2-hydroxyphenylmethyl)]-[(2-pyridinyl)methyl]-1,3-propanediamine, 15 mL of dichloromethane, and 187 mg of Fe@MWCNT-Cl were introduced and refluxed under inert atmosphere for 96 hours. The postreaction mixture was filtered using a fritted funnel with a PTFE filter and washed with ethanol. The resulting semisolid was dried under reduced pressure, yielding 825 mg of dry product.

Fe@f-MWCNT

Fe@MWCNTs (87 mg) and 1,1,2,2-tetrachloroethane (40 mL) were placed in a 100 mL round-bottom flask. The dispersion was sonicated for 1 hour at room temperature. Then, a solution of p-azidophenol (121 mg, 0.9 mmol) in 1,1,2,2-dichloroethane (10 mL) was added, and the resulting mixture was refluxed for 8 hours under nitrogen atmosphere. The solid product was filtered over a PTFE membrane filter (0.45-μm pore size) and washed thoroughly with chloroform (150 mL), methanol (150 mL), and toluene (150 mL). Subsequent drying (24 hours at 100°C) resulted in 102 mg of the product.

Fe³⁺ anchoring

Iron(III) stock solution was prepared by dissolving anhydrous iron(III) chloride in demineralized water, resulting in a solution of 4.3 mg cm⁻³ (26 mM) concentration. Typical procedure of iron(III) anchoring on Fe@MWCNTs exemplified on the synthesis of Fe(III)/Fe@O-MWCNT was as follows: the mixture of 100 mg of Fe@O-MWCNT and 50 mL of the iron(III) stock solution was sonicated for 3 hours. After 24 hours of free sedimentation, the dispersion was centrifuged at 10,000 rpm for 30 minutes. The supernatant was decanted and 50 mL of demineralized water was added to the precipitate. The washing procedure was repeated three times, resulting in iron(III)-free supernatant (rhodanide test). The precipitate was finally transferred with new batch of water to the lyophilization process, yielding 92 mg of dry product (Fe(III)/Fe@O-MWCNT).

Studies on the stability of hybrid dispersions

The sedimentation measurements were carried out on dispersions of 0.5 mg Fe@MWCNTs in 5 mL of demineralized water ultrasonicated for 1 hour. An aliquot (4 mL) of this suspension was transferred to a quartz UV cell, and UV–Vis measurements were taken within 24 hours.

Conclusion

New magnetically active Fe–nanotube hybrids were obtained. The hybrids expressed moderate relaxivities r_2, but Fe^{3+} anchoring enhanced and even tripled the relaxivity values after coordination, which falls within the range of commercial T_2 CAs. Fe@MWCNTs offer versatility of physicochemical modifications and biocompatibility, and they have already gained prominence due to their efficiency in crossing the blood–brain barrier.[49] Nevertheless, there are several factors that should be taken into account while proposing CNT candidates for applications as MRI CAs. One of the most important ones is effectiveness of relaxation in a given strength of magnetic field. Because many gadolinium derivatives are efficient in low fields (1.0–1.5 T), there is a demand for new CAs for high-field modern tomographs. The proposed methodology of MWCNTs' functionalization, followed by the amalgamation with Fe^{3+} ion, is attractive because it opens new possibilities leading to materials that are highly efficient in the acceleration of proton relaxation. Apart from the assessment of basic morphological, physical, and chemical properties of the hybrids (stability of the dispersions, uniformity of raw and functionalized materials, etc), biodistribution, cytotoxicity, and in vivo production of contrast will be the deciding factors. As the hybrids are built on a new, exogenous material, it is not surprising that they raise concern in the medical environment. Particular care should be taken in the comprehensive in vivo studies of the materials.

Acknowledgments

Disclosure

The authors report no conflicts of interest in this work.

References

1. Radushkevich LV, Lukyanovich VM. O strukture ugleroda, obrazujucegosja pri termiceskom razlozenii okisi ugleroda na zeleznom kontakte. *Zurn Fisic Chim*. 1952;26:88–95.
2. Iijima S. Helical microtubules of graphitic carbon. *Nature*. 1991; 354(6348):56–58.
3. Devadasu VR, Bhardwaj V, Kumar MNVR. Can controversial nanotechnology promise drug delivery? *Chem Rev*. 2012;113(3): 1686–1735.
4. De Volder MFL, Tawfick SH, Baughman RH, Hart AJ. Carbon nanotubes: present and future commercial applications. *Science*. 2013;339(6119):535–539.
5. Du J, Wang S, You H, Zhao X. Understanding the toxicity of carbon nanotubes in the environment is crucial to the control of nanomaterials in producing and processing and the assessment of health risk for human: a review. *Environ Toxicol Pharmacol*. 2013;36(2): 451–462.
6. Liu Y, Zhao Y, Sun B, Chen C. Understanding the toxicity of carbon nanotubes. *Acc Chem Res*. 2012;46(3):702–713.
7. Heister E, Brunner EW, Dieckmann GR, Jurewicz I, Dalton AB. Are carbon nanotubes a natural solution? Applications in biology and medicine. *ACS Appl Mater Interfaces*. 2013;5(6):1870–1891.
8. Kostarelos K, Bianco A, Prato M. Promises, facts and challenges for carbon nanotubes in imaging and therapeutics. *Nat Nanotechnol*. 2009;4(10):627–633.
9. Sethi R, Mackeyev Y, Wilson LJ. The gadonanotubes revisited: a new frontier in MRI contrast agent design. *Inorganica Chim Acta*. 2012;393:165–172.
10. Bloembergen N. Proton relaxation times in paramagnetic solutions. *J Chem Phys*. 1957;27:572–580.
11. Singh C, Shaffer MSP, Koziol KKK, Kinloch IA, Windle AH. Towards the production of large-scale aligned carbon nanotubes. *Chem Phys Lett*. 2003;372(5):860–865.
12. Boncel S, Pattinson SW, Geiser V, Shaffer MSP, Koziol KKK. En route to controlled catalytic CVD synthesis of densely packed and vertically aligned nitrogen-doped carbon nanotube arrays. *Beilstein J Nanotechnol*. 2014;5(1):219–233.
13. Karousis N, Tagmatarchis N, Tasis D. Current progress on the chemical modification of carbon nanotubes. *Chem Rev*. 2010;110(9): 5366–5397.
14. Kuźnik N, Tomczyk MM, Boncel S, Herman AP, Koziol KKK, Kempka M. Fe3+ ions anchored to Fe@O-MWCNTs as a double impact T2 MRI contrast agents. *Mater Lett*. 2014;136:34–36.
15. Hong H, Gao T, Cai W. Molecular imaging with single-walled carbon nanotubes. *Nano Today*. 2009;4(3):252–261.
16. Liu Z, Yang K, Lee ST. Single-walled carbon nanotubes in biomedical imaging. *J Mater Chem*. 2011;21(3):586–598.
17. Sitharaman B, Kissell KR, Hartman KB, et al. Superparamagnetic gadonanotubes are high-performance MRI contrast agents. *Chem Commun*. 2005;(31):3915–3917.
18. Sitharaman B, Van Der Zande M, Ananta JS, et al. Magnetic resonance imaging studies on gadonanotube-reinforced biodegradable polymer nanocomposites. *J Biomed Mater Res A*. 2010;93(4):1454–1462.
19. Ananta JS, Matson ML, Tang AM, Mandal T, Lin S, Wong KK. Singlewalled carbon nanotube materials as T2-weighted MRI contrast agents. *J Phys Chem C*. 2009;113:19369–19372.
20. Miyawaki J, Yudasaka M, Imai H, et al. In vivo magnetic resonance imaging of single-walled carbon nanohorns by labeling with magnetite nanoparticles. *Adv Mater*. 2006;18(8):1010–1014.
21. Choi JH, Nguyen FT, Barone PW, et al. Multimodal biomedical imaging with asymmetric single-walled carbon nanotube/iron oxide nanoparticle complexes. *Nano Lett*. 2007;7(4):861–867.
22. Doan BT, Seguin J, Breton M, et al. Functionalized single-walled carbon nanotubes containing traces of iron as new negative MRI contrast agents for in vivo imaging. *Contrast Media Mol Imaging*. 2012;7(2):153–159.
23. Jahanbakhsh R, Atyabi F, Shanehsazzadeh S, Sobhani Z, Adeli M, Dinarvand R. Modified gadonanotubes as a promising novel MRI contrasting agent. *DARU*. 2013;21(6):53–61.
24. Yin M, Wang M, Miao F, et al. Water-dispersible multiwalled carbon nanotube/iron oxide hybrids as contrast agents for cellular magnetic resonance imaging. *Carbon N Y*. 2012;50:2162–2170.
25. Ding X, Singh R, Burke A, et al. Development of iron-containing multiwalled carbon nanotubes for MR-guided laser-induced thermotherapy. *Nanomedicine*. 2011;6(8):1341–1352.
26. Wu H, Liu G, Zhuang Y, et al. The behavior after intravenous injection in mice of multiwalled carbon nanotube/Fe3O4 hybrid MRI contrast agents. *Biomaterials*. 2011;32(21):4867–4876.
27. Liu Y, Hughes TC, Muir BW, et al. Water-dispersible magnetic carbon nanotubes as T2-weighted MRI contrast agents. *Biomaterials*. 2014;35:378–386.
28. Richard C, Doan BT, Beloeil JC, Bessodes M, Tóth E, Scherman D. Noncovalent functionalization of carbon nanotubes with amphiphilic Gd3+ chelates: toward powerful T1and T2 MRI contrast agents. *Nano Lett*. 2008;8(1):232–236.
29. Boncel S, Müller KH, Skepper JN, Walczak KZ, Koziol KK. Tunable chemistry and morphology of multi-wall carbon nanotubes as a route to non-toxic, theranostic systems. *Biomaterials*. 2011;32: 7677–7686.
30. Ali-Boucetta H, Kostarelos K. Pharmacology of carbon nanotubes: toxicokinetics, excretion and tissue accumulation. *Adv Drug Deliv Rev*. 2013;65(15):2111–2119.
31. Ali-Boucetta H, Nunes A, Sainz R, et al. Asbestos-like pathogenicity of long carbon nanotubes alleviated by chemical functionalization. *Angew Chem Int Ed*. 2013;125(8):2330–2334.
32. Boncel S, Koziol KKK, Walczak KZ, Windle AH, Shaffer MSP. Infiltration of highly aligned carbon nanotube arrays with molten polystyrene. *Mater Lett*. 2011;65(14):2299–2303.
33. Hong T, Lazarenko RM, Colvin DC, Flores RL, Zhang Q, Xu YQ. Effect of competitive surface functionalization on dual-modality fluorescence and magnetic resonance imaging of single-walled carbon nanotubes. *J Phys Chem C*. 2012;116(30):16319–16324.
34. Han J, Gao C. Functionalization of carbon nanotubes and other nanocarbons by azide chemistry. *Nano-Micro Letters*. 2010;2(3):213–226.
35. McCleverty JA, Meyer TJ, Lever ABP. *Comprehensive Coordination Chemistry II: from Biology to Nanotechnology*. Amsterdam: Elsevier; 2004.
36. Abuilaiwi FA, Laoui T, Al-Harthi M, Atieh MA. Modification and functionalization of multiwalled carbon nanotube (MWCNT) via fischer esterification. *Arab J Sci Eng*. 2010;35(1C):37–48.
37. Silverstein RM, Webster F, Kiemle D, Bryce DL. *Spectrometric Identification of Organic Compounds*. (8th Ed., ed.). Hoboken, NJ: John Wiley & Sons; 2014.
38. Chen J, Hamon MA, Hu H, et al. Solution properties of single-walled carbon nanotubes. *Science*. 1998;282(5386):95–98.
39. Hureau C, Anxolabéhère-Mallart E, Blondin G, Rivière E, Nierlich M. Synthesis, structure and characterisation of a new trinuclear Di-μ-phenolato-μ-carboxylato MnIIIMnIIMnIII complex with a bulky pentadentate ligand: chemical access to mononuclear MnIV-OH entities. *Eur J Inorg Chem*. 2005;2005(23):4808–4817.
40. Belloli R. Nitrenes. *J Chem Educ*. 1971;48(7):422–426.
41. Cheng X, Zhong J, Meng J, et al. Characterization of multiwalled carbon nanotubes dispersing in water and association with biological effects. *J Nanomater*. 2011;2011:1–12.
42. Marangon I, Ménard-Moyon C, Kolosnjaj-Tabi J, et al. Covalent functionalization of multi-walled carbon nanotubes with a gadolinium chelate for efficient T1-weighted magnetic resonance imaging. *Adv Funct Mater*. 2014;24(45):7173–7186.

43. De León-Rodríguez LM, Viswanathan S, Sherry AD. A study on the synthesis and properties of substituted EHBG-Fe (III) complexes as potential MRI contrast agents. *J Organomet Chem*. 2014;769:100–105.

44. Kuźnik N, Jewuła P, Oczek L, Kozłowicz S, Grucela A, Domagała W. EHPG iron(III) complexes as potential contrast agents for MRI. *Acta Chim Slov*. 2014;61:87–93.

45. Welsher K, Liu Z, Sherlock SP, et al. A route to brightly fluorescent carbon nanotubes for near-infrared imaging in mice. *Nat Nanotechnol*. 2009;4(11):773–780.

46. Chen B, Zhang H, Du N, et al. Magnetic-fluorescent nanohybrids of carbon nanotubes coated with Eu, Gd Co-doped LaF3 as a multimodal imaging probe. *J Colloid Interface Sci*. 2011;367(1):61–66.

47. Bai X, Son SJ, Zhang S, et al. Synthesis of superparamagnetic nanotubes as MRI contrast agents and for cell labeling. *Nanomedicine*. 2008;3(2):163–174.

48. Hartman KB, Laus S, Bolskar RD, et al. Gadonanotubes as ultrasensitive pH-smart probes for magnetic resonance imaging. *Nano Lett*. 2008;8(2):415–419.

49. Ren J, Shen S, Wang D, et al. The targeted delivery of anticancer drugs to brain glioma by PEGylated oxidized multi-walled carbon nanotubes modified with angiopep-2. *Biomaterials*. 2012;33(11):3324–3333.